Chapter 4
Numerical Studies of Gas-particle Flow over a Backward Facing Step and in a 90-degree Bend

This chapter describes the numerical investigation of the turbulent gas-particle flow over a backward facing step and the turbulent gas-particle flow through a 90º bend, using both the Eulerian-Eulerian model in described in Chapter 3.2.1 and the Eulerian-Lagrangian model described in Chapter 3.2.2. In the framework of the Lagrangian model, the discrete random walk (DRW) model in the generic CFD code FLUENT was employed here. Tu and Fletcher (1995) established a set of Eulerian formulation with generalised wall boundary conditions and developed a particle-wall collision model to better represent the particle-wall momentum transfer. This set of Eulerian formulation has been implemented in an in-house Eulerian-Eulerian CFD code and used in this study.

4.1 Turbulent gas-particle flow over a backward facing step

The backward facing step (see Figure 4.1) presents one of the basic geometry in many engineering applications where the presence of turbulent flow over the backward facing step allows the determination and fundamental understanding of important flow features such as flow separation, flow reattachment and free shear jet phenomena. Tremendous numerical and experimental studies of gas-particle flow over the backward facing step have been reported in literature. However, to the best of the authors' knowledge, no in-depth investigations have been performed on the comparison of the Eulerian-Eulerian model and Eulerian-Lagrangian model performance with measurements on the benchmark problem of gas-particle flow over a backward facing step problem. Hallman et al. (1995) focused on the computation of turbulent evaporating sprays using the Eulerian and Lagrangian approaches. Recently, Lee et al. (2002) simulated the gas-particle flow in a 45° ramp and an isolated single tube using Eulerian-Lagrangian and Eulerian-Eulerian methods and both approaches have been found to yield good agreement with measured results. Bourloutski et al. (2002) later verified both approaches in turbulent gas-particle flows with heat transfer in a pipe.

In this part, the turbulent gas-particle flow over backward facing step were simulated using both a Lagrangian particle tracking model (DRW model) and an Eulerian two-fluid model with overlapped grid system (Tu, 1997). The simulation results were validated against experimental data obtained by Ruck et al. (1988).

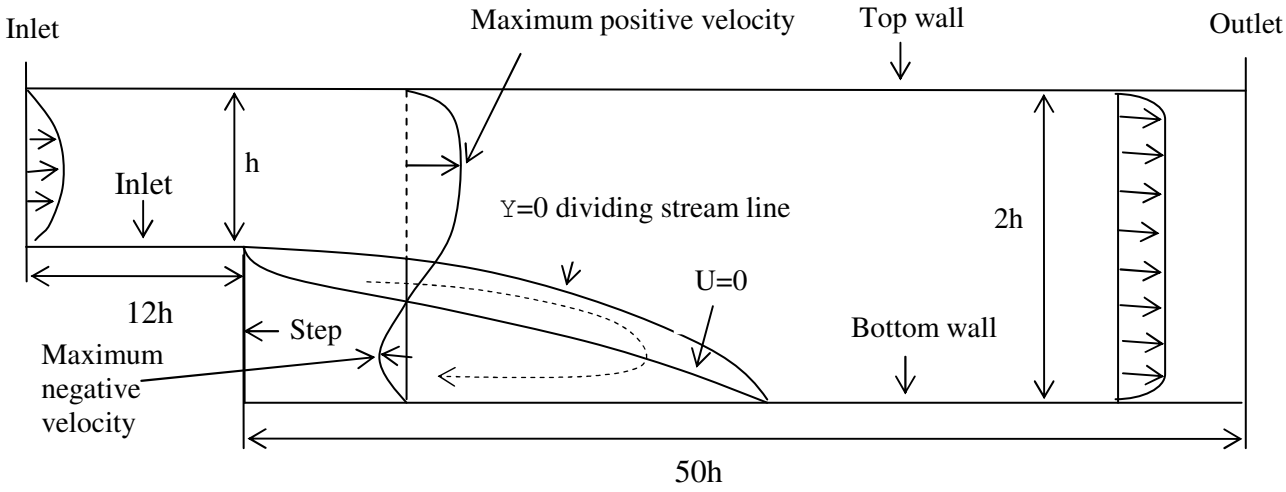

Figure 4.1 Schematic drawing of the backward facing step geometry (h = 0.025m)

4.1.1 Numerical procedure

Particles with corresponding diameters of 1 μm (ρ_p = 810 kg/m^3) and 70 μm (ρ_p = 1500 kg/m^3) were simulated under the flow condition of two Reynolds numbers (based on the step height h): *Re* = 64000 and *Re* = 15000. The numerical exercise was performed in a two-dimensional (2D) environment since only 2D representative measurements are available.

The governing transport equations were discretised using the finite-volume approach. Third order QUICK scheme was used to approximate the convective terms while second order accurate central differencing scheme was adopted for the diffusion terms. The pressure-velocity coupling was realized through the SIMPLE method. The simulations were marched towards steady state.

For the Lagrangian particle tracking model, a computational domain has a size of 12h × 1h before the step and 50 h × 2 h after the step to ensure the flow was fully developed at the exit. Within the length of 12 h before the step, 120 (in the streamwise direction) × 20 (in the lateral direction) uniform grid points have been allocated. Further downstream, the mesh is with 500 uniform grid points in the streamwise direction and 40 uniform grid points in the lateral direction. Grid independence was checked by refining the mesh system through doubling the number of grid points along the streamwise and 50 uniform grid points in the lateral directions. Simulations using RNG k-ε model revealed that the difference of the reattachment length between the two mesh schemes is less than 3%. The coarser mesh was therefore applied in order to embrace the increase of computational efficiency towards achieving the final results. The convergence criteria for the gas phase properties (velocities, pressure, k and ε) were achieved when the iteration residuals reduced by six order of magnitude. The Non-Equilibrium wall function was employed for the gas phase flow because of its capability to better handle complex flows where the mean flow and turbulence are subjected to severe pressure gradients and rapid change, such as separation, reattachment and impingement. The distance *y*+ is a dimensionless parameter defined as $y^+ = \frac{\rho_g u_T y_P}{\mu_g}$. Here, $u_T = \sqrt{\tau_\omega / \rho_g}$ is the friction velocity, y_p is the distance from point P to the wall, τ_ω is the wall shear stress, and μ_g is the fluid viscosity at point P. The ranges of y+ of boundary cells along the top wall, bottom wall and inlet bottom wall (see Figure 4.1) investigated are listed in Table 4.1. Figure 4.2 depicts the distribution of *y*+ obtained by the RNG k-ε model. It was observed that in the recirculation region and recovering region, low values of *y*+ were found along the bottom wall.

Wall	RNG k-ε model	Realizable k-ε model	Standard k-ε model
Top wall	35<y+<81	31<y+<81	37<y+<81
Bottom wall	2<y+<45	2 <y+<47	2<y+<45
Inlet bottom	59<y+<73	59<y+<79	75<y+<59

Table 4.1 y+ of boundary cells along the top wall, bottom wall and inlet bottom wall.

The particle transport using the DRW model was computed from the converged solution of the gas flow. For the DRW model, a total of 20000 particles were released from 10

uniformly distributed points across the inlet and they were individually tracked within the backward facing step geometry. The independence of statistical particle phase prediction from the increase of particle number was tested using 10,000, 20,000 and 50,000 particles for 70 μm. The difference of the maximum positive velocities of 20,000 and 50,000 particles was less than 1%.

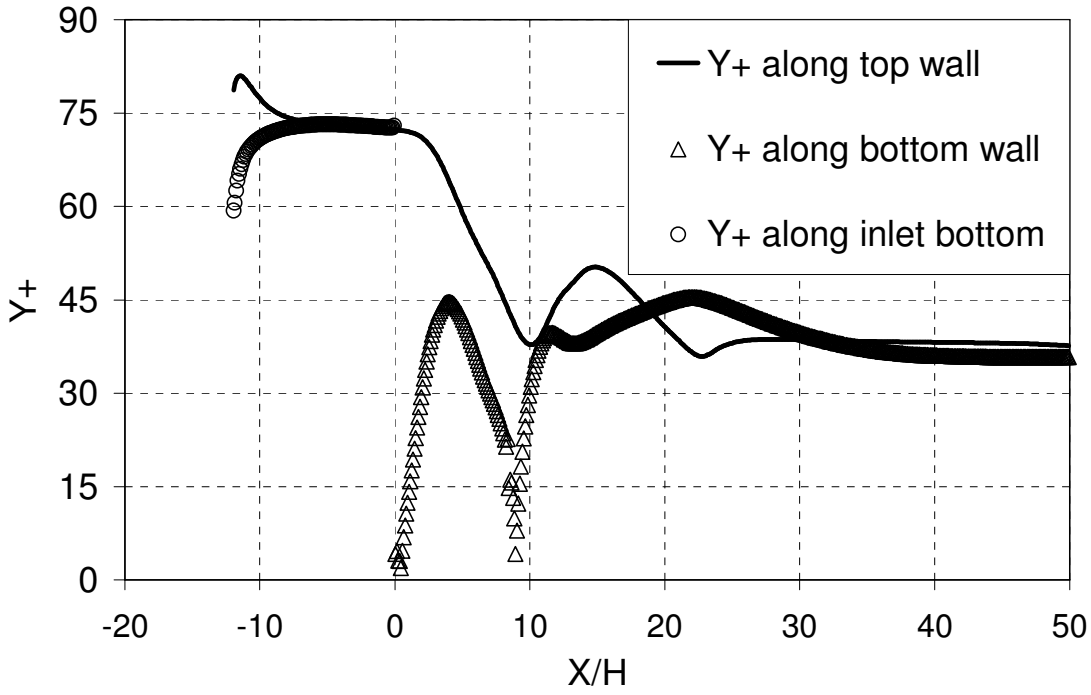

Figure 4.2 Distribution of y+ of boundary cells (RNG k-ε model)

For the Eulerian two-fluid model, computations were performed using an overlapped grid system with three computational zones: 100 (in the streamwise direction) and 60 (in the lateral direction) uniform grid points are allocated for the region of x/h = 10 behind the step. There are a total of 162 grids in the streamwise direction, while three grids in the span-wise direction that comprise two symmetric walls. All the transport equations for both phases were discretized by a finite-volume formulation using an overlapped grid system. The QUICK scheme was used for the convective terms, while three-point symmetric formulas were used for the second-order derivatives. The SIMPLE algorithm was used for the velocity-pressure coupling. More details the overlapped grid system can be found in Tu (1997).

All the calculations were performed on a PC workstation having the following hardware specifications: 2.66 GHz CPU and 512 Mega-bytes of RAM. To investigate the computational performance for Lagrangian and Eulerian approaches, CPU times for both of the methods were recorded and normalized with the CPU time for Eulerian model in the case of Re = 15000, d_p = 70 μm. Table 4.2 illustrates the normalized CPU time for Lagrangian model using 20,000 particles and 50,000 particles accompanied by the CPU time for the Eulerian model. The CPU times described here comprise both the convergence time for the gas phase and the calculation time for the particles phase. It clearly demonstrated that more computational time is required for the Lagrangian approach than the Eulerian approach.

Model	Case	Normalized CPU time	Grid
Lagrangian (20,000 particles)	Re=15000, d_p=1μm	1.75	500×40×1 +120×20×1 =22400
	Re=15000, d_p=70μm	1.7	
Lagrangian (50,000 particles)	Re=15000 d_p=70μm	3.3	
	Re=64000, d_p=70μm	3.2	
Eulerian	Re=15000, d_p=1μm	1.15	162×60×3 =29160
	Re=15000, d_p=70μm	1	
	Re=64000, d_p=1μm	1.15	
	Re=64000, d_p=70μm	1	

Table 4.2 Normalized CPU times of Eulerian-Lagrangian and Eulerian-Eulerian approaches

4.1.2 Results and discussions

For gas-particle flows, the dimensionless number – Stokes number, which is defined as the ratio between the particle relaxation time and system response time, i.e. $St = \tau_p/t_s$, presents an important criteria towards understanding the state of the particles whether they are in kinetic equilibrium with the surrounding gas. The system relaxation time τ_p in the Stokes number definition has been determined from the characteristic length (L_s) and the characteristic velocity (V_s) of the system under investigation, i.e. $t_s = L_s / V_s$.

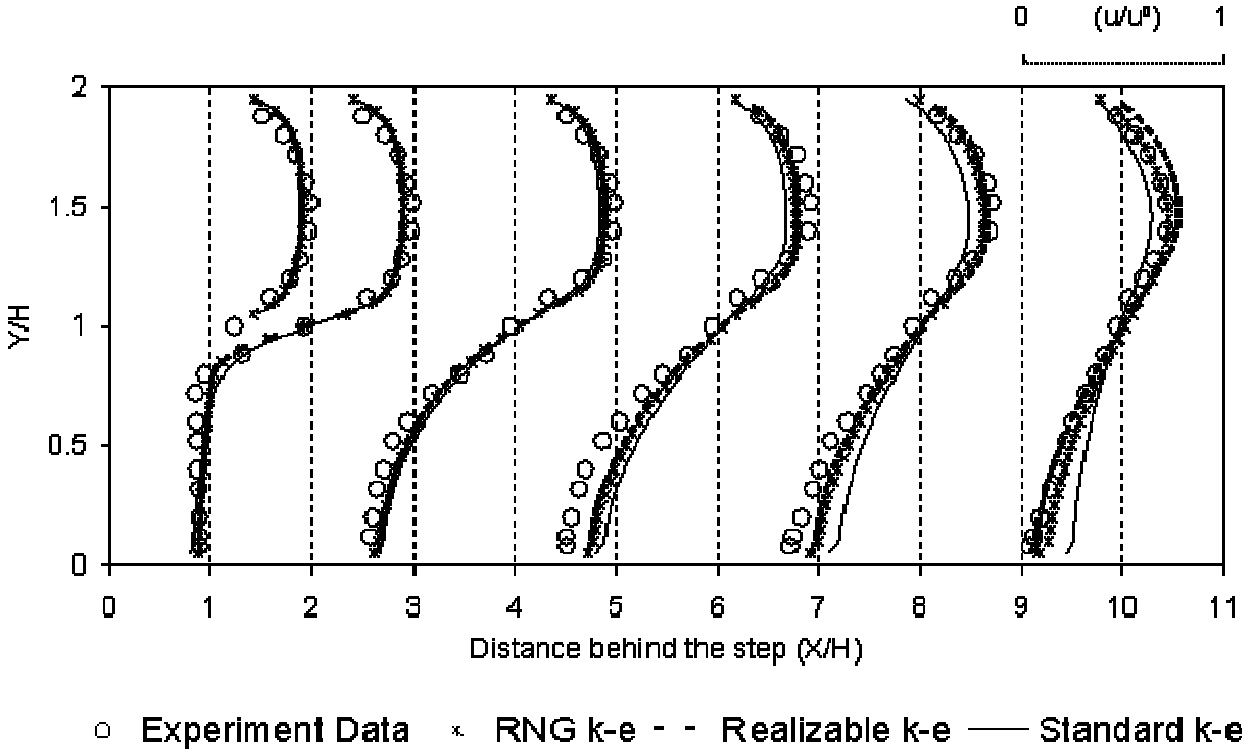

(a)

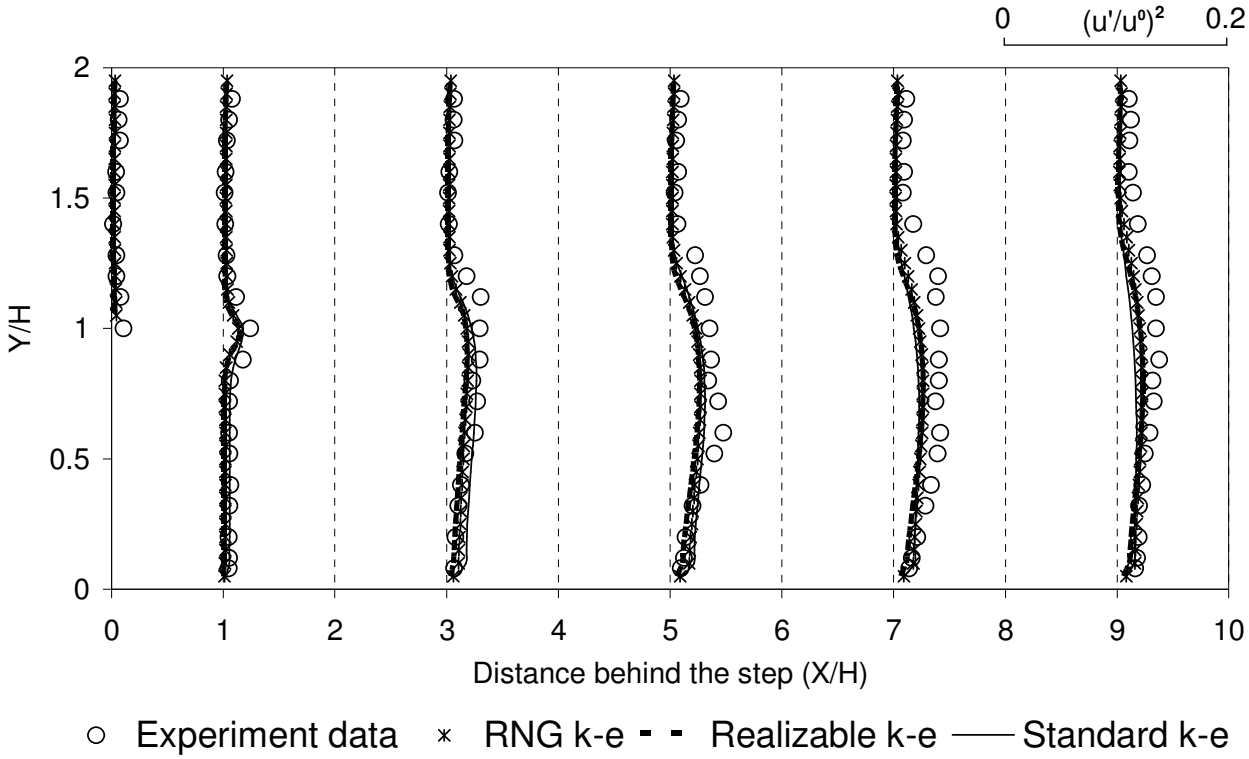

(b)

Figure 4.3 Comparison between the experimental data and numerical simulation of (a) particle velocities, (b) particle turbulent fluctuations (Re = 64000, d_p = 1 μm)

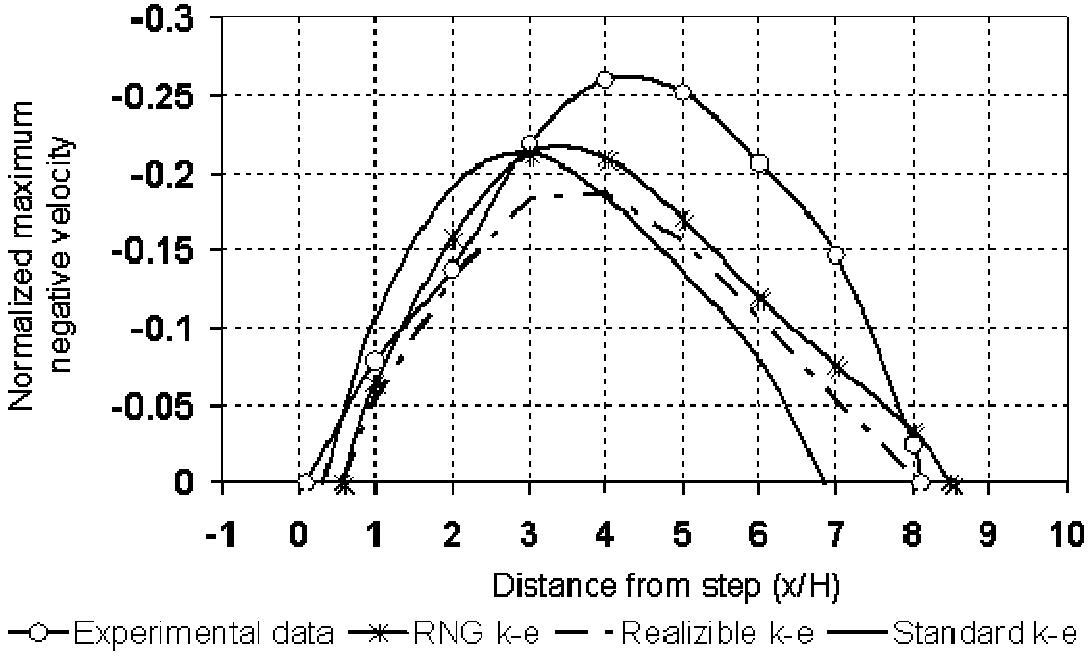

Figure 4.4 Maximum negative velocity U-max (normalized with free stream velocity Uo) in the recirculation zone of particles of different k-ε models (Re = 64000, d_p = 1 μm)

For the case of particles with a diameter size of 1μm (categorized as small particles) with gas flows of Reynolds numbers of 15000 and 64000, the Stokes numbers evaluated for these particles were found to be very much less than unity. This particle flow could be considered to act more like fluid traces in the gas flow, which provided the necessary means of assessing the prediction accuracy of the gas phase turbulent models since they played an important role in affecting the particle flow across the backward facing step geometry. A parametric study was performed using three available turbulent k-ε models in FLUENT: standard k-ε, realizable k-ε and RNG k-ε whilst employing the Lagrangian particle tracking model. Figure 4.3(a) presents the computed particle velocity profiles against measurements for a Reynolds number of 64000, at locations of x/H = 0, 1, 3, 5, 7 and 9 respectively behind the step. The velocity profiles are normalized by the free stream velocity u_0 that is with value of 40 m/s. Good agreement was achieved with the realizable k-ε and RNG k-ε models while significant deviations were found employing the standard k-ε model at downstream locations of x/H = 5, 7 and 9. Figure 4.3(b) gives the comparison of predicted and measured particle turbulent fluctuation. The predicted particle turbulent fluctuations downstream of x/H=3 are lower than the experiment data. Under the same flow condition, the maximum negative velocity profiles of the particles in the recirculation

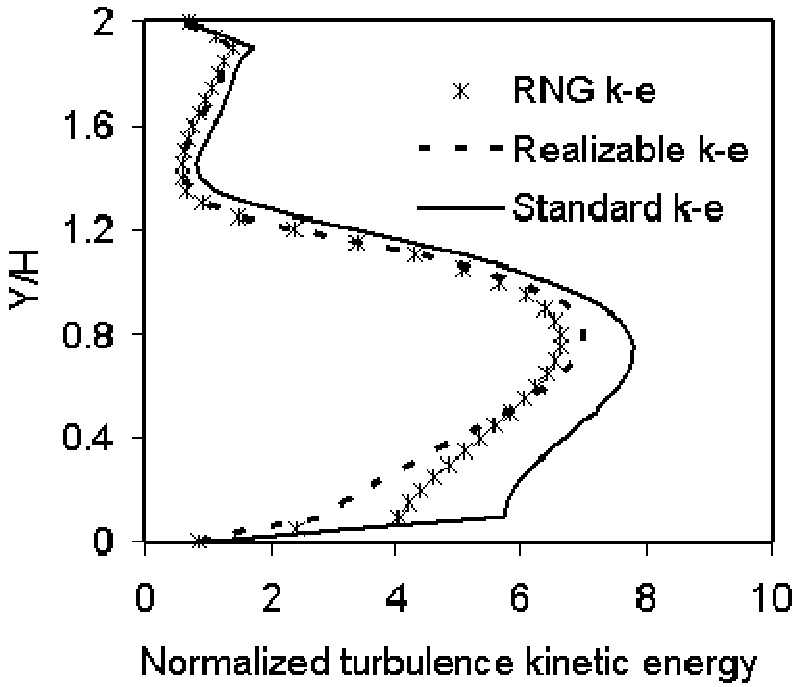

(a)

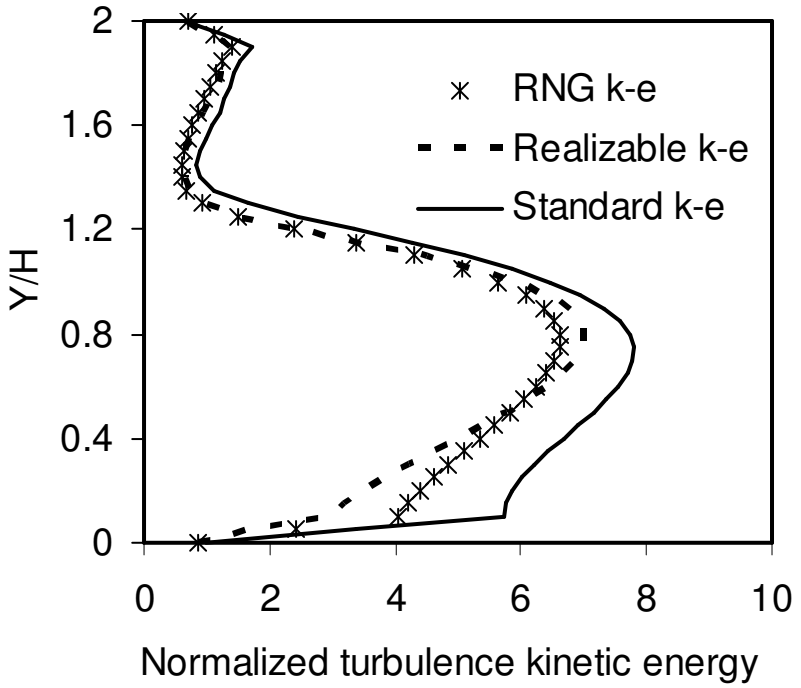

(b)

Figure 4.5 (a) the computed turbulent kinetic energy k (normalized by the inlet mean k) at x/H=5, (b) the computed turbulent dissipation rate ε (normalized by the inlet mean ε) at x/H=5

zone are illustrated in Figure 4.4. All the three turbulent models yielded lower maximum values of the maximum negative velocities. Nevertheless, the realizable k-ε model gave the best prediction of the particle reattachment length of x/H = 8.2 comparing to the measured value of x/H = 8.1 while the standard k-ε model severely under predicted the reattachment length by value of x/H = 6.9. The RNG k-ε model predicted the particle reattachment length of x/H = 8.5.

The standard k-ε model generally over predicts the gas turbulence kinetic energy k in the recirculation region, which leads to a high turbulent viscosity $\nu_{g,t}$. Figure 4.5 (a) demonstrates the profile of the turbulent kinetic energy k normalised by the mean k at inlet at location of X/h = 5 while Figure 4.5 (b) provides the profile of the turbulent dissipation rate ε normalised by the mean ε at inlet at the identical location. It is evidently clear that the standard k-ε model yielded excessive normalised turbulent kinetic energy k values while the predicted normalised turbulent dissipation rate ε values at the same locations were, however, just marginally higher below the step height of 0.025 m. This therefore resulted in the over prediction of $\nu_{g,t}$ and the production of excessive mixing in the standard k-ε model, which significantly reduced the recirculation zone (confirmed also through Murakami, 1993). Another possible cause could be the ε transport equation of the standard k-ε model. For example, in the RNG k-ε model, additional term such as a strain dependent term *R* is included to aid the model in dealing with flows that experience large rates of deformation (Wright, 2003). In Equation (3.19), it can be observed that in regions where $\eta < \eta_0$, R is positive. When $\eta > \eta_0$, *R* turns negative. The negative value of R decreases both the rate of production of k and rate of destruction of ε, leading to smaller eddy viscosity (Orzag, 1994). For rapidly strained flows, the RNG k-ε model yields a lower turbulent viscosity than the standard k-ε model. Figure 4.6 illustrates the turbulent viscosity profiles obtained by three models. It is clearly seen that the standard k-ε model predicts much higher $\nu_{g,t}$ than the other two models in the region from X/H = 3.5 to X/H = 7.3 and in the region downstream X/H = 9.

Figure 4.7(a) and (b) present the velocity profile of particles with diameter size of 70 μm (large particles), in the flows of Re = 64000 and Re = 15000, respectively. Here, the larger particle results have been obtained via the Eulerian-Lagrangian model. Since the Stokes number is much greater than one, the fluency from the fluid phase fluctuations the particles

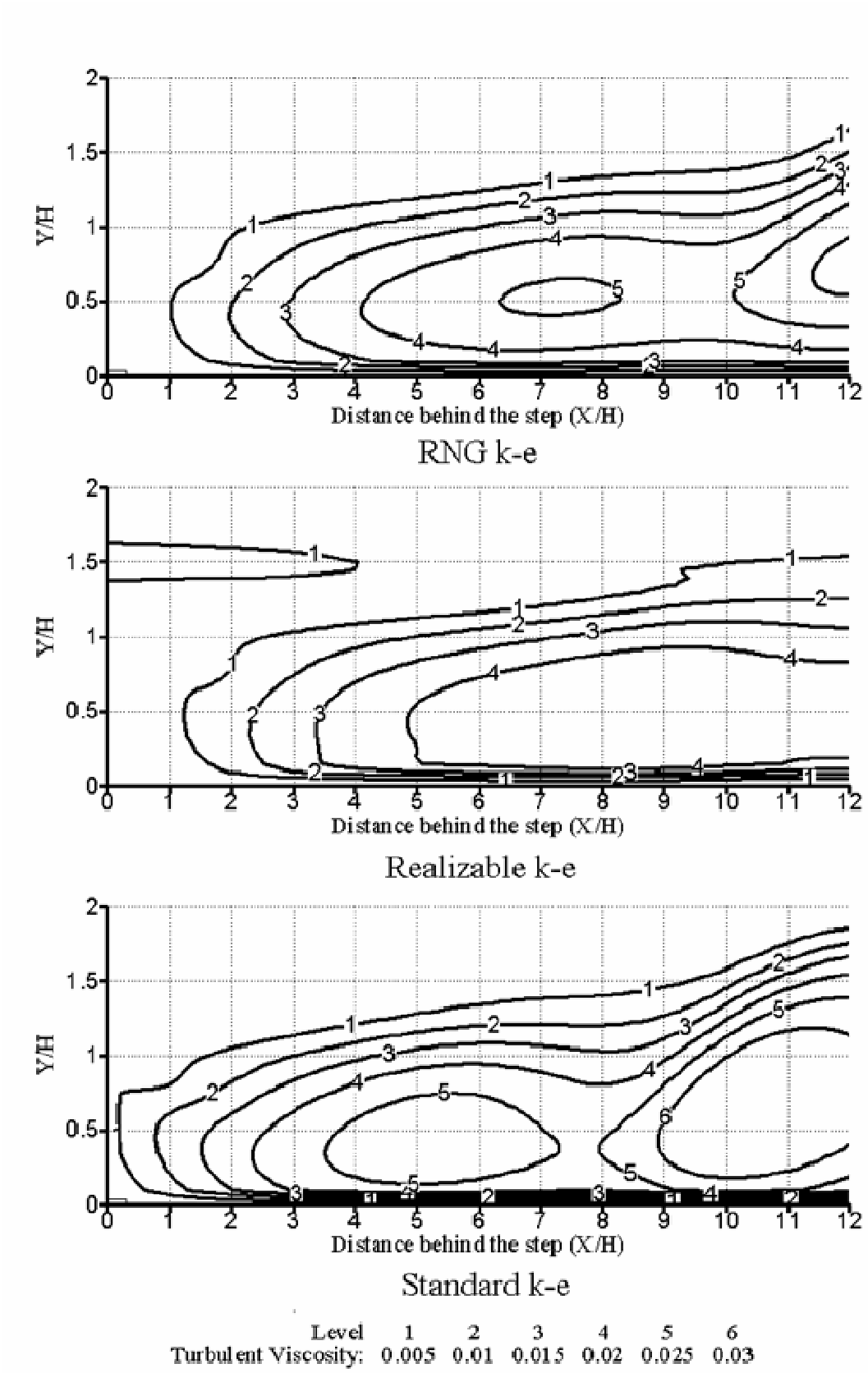

Figure 4.6 The turbulent viscosity profiles predicted by three models

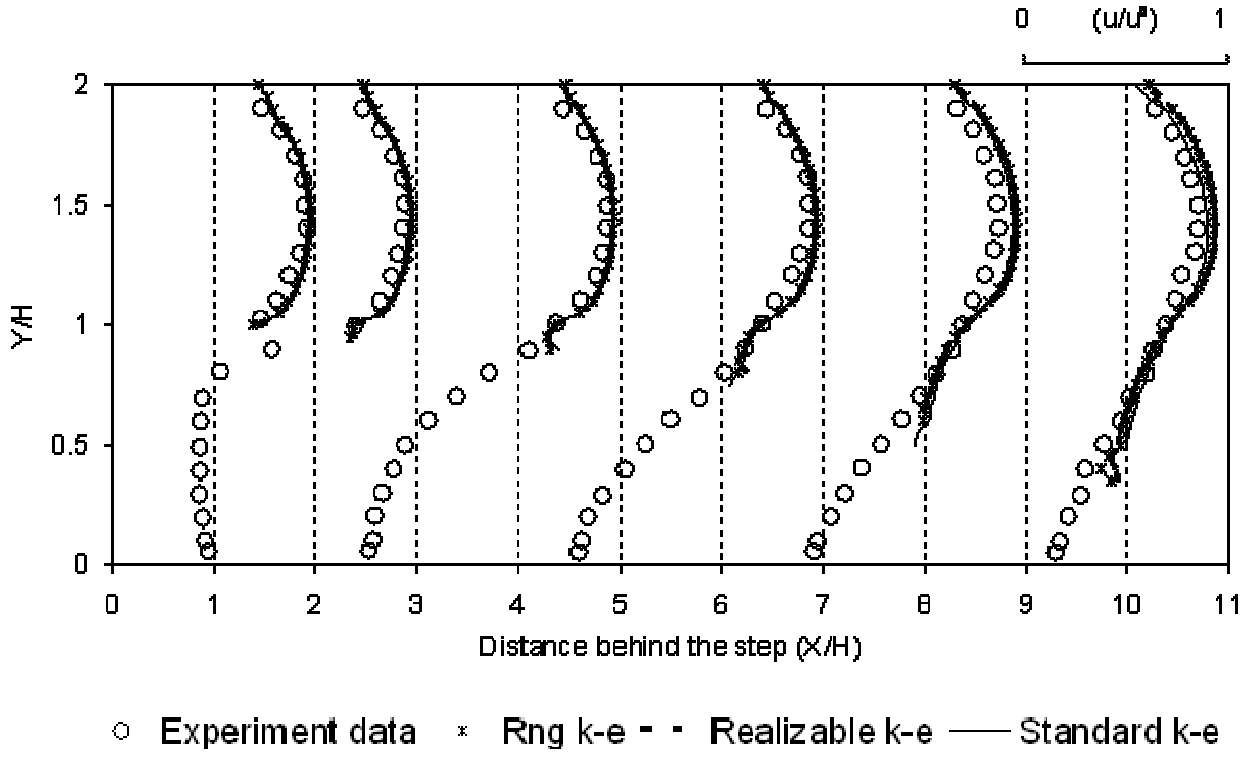

(a)

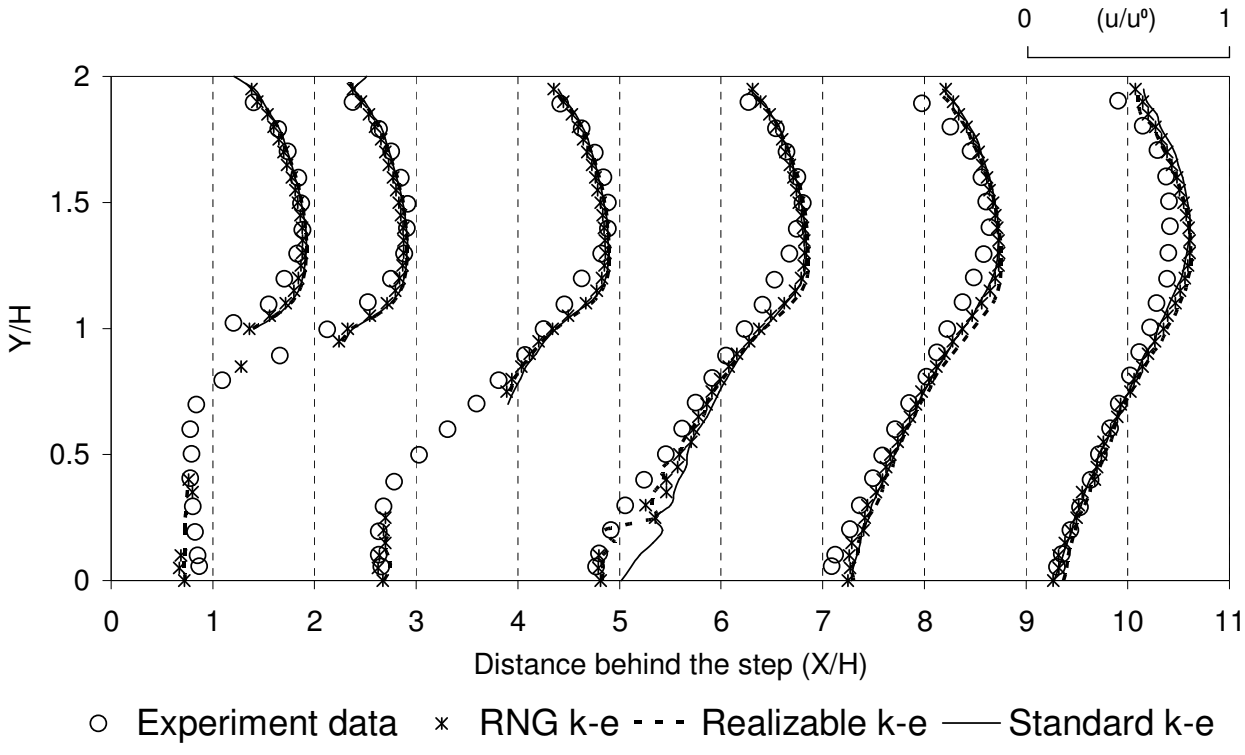

(b)

Figure 4.7 Comparison between the experimental data and numerical simulation of particle velocities: (a) Re=64000, (b) Re=15000 (d_p = 70 μm)

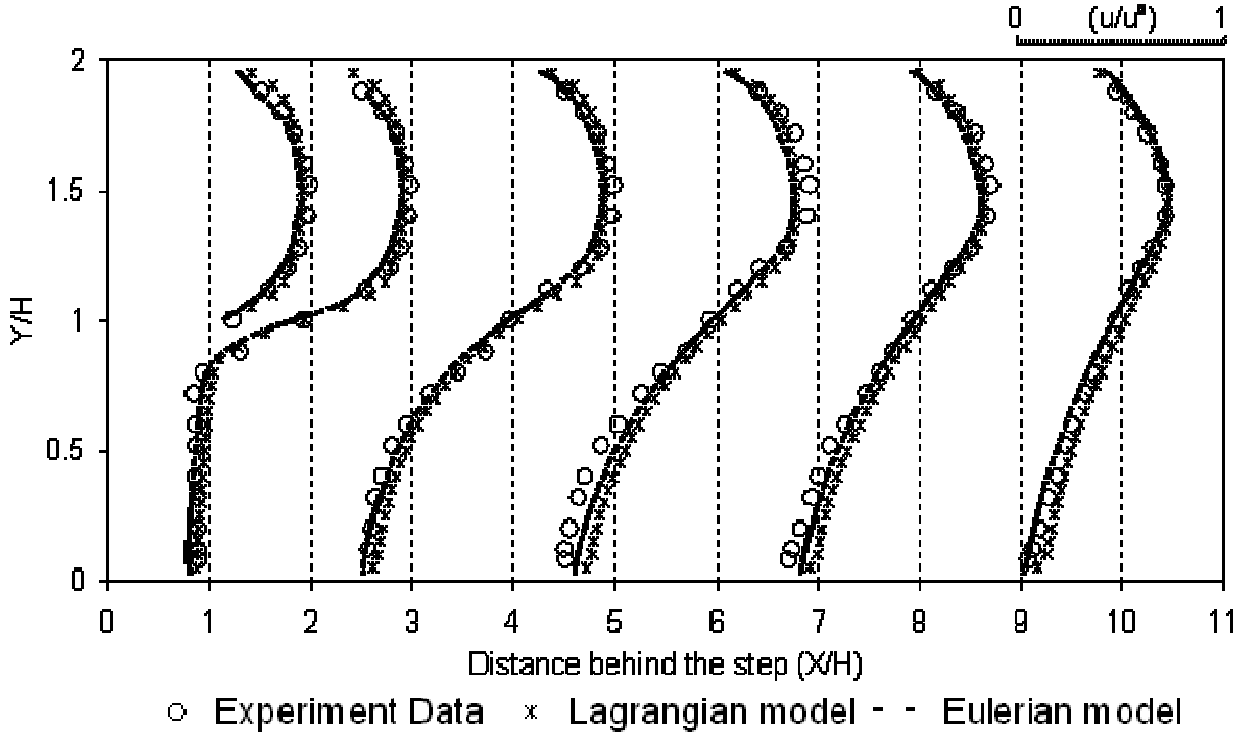

(a)

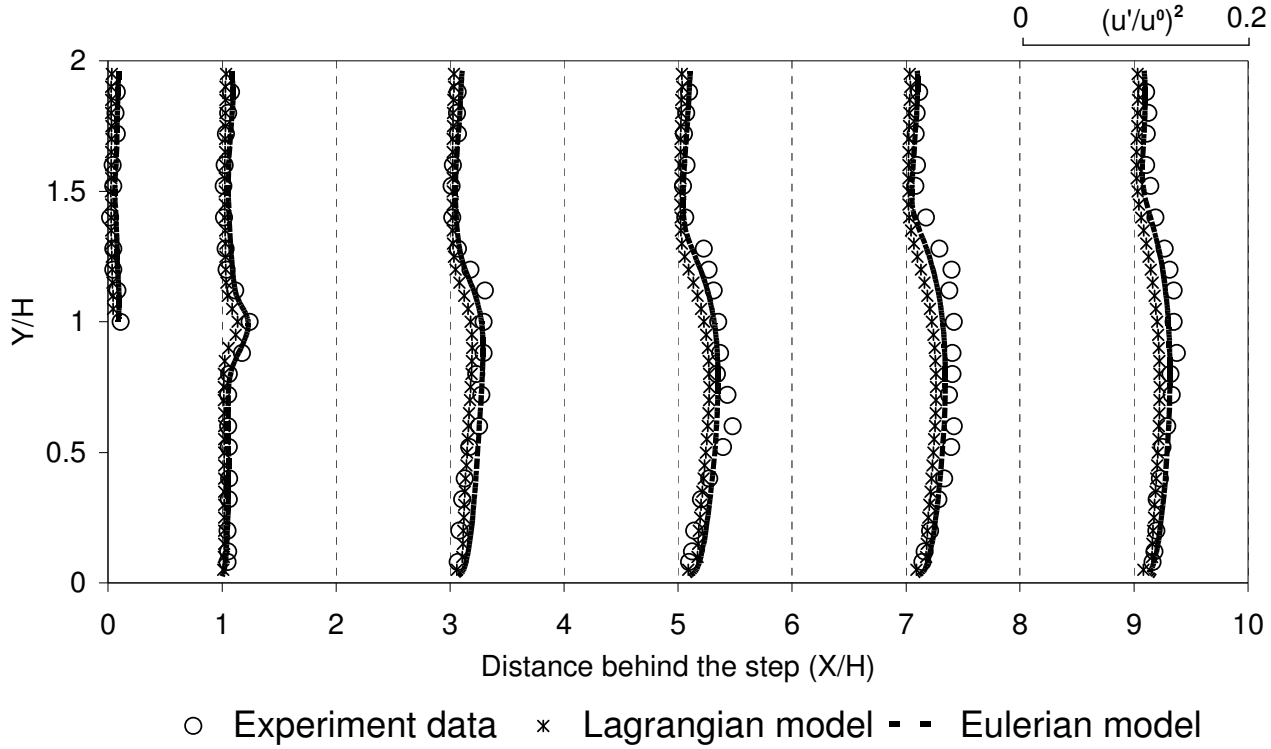

(b)

Figure 4.8 Comparison between the experimental data and numerical simulation results with Lagrangian and Eulerian models: (a) particle velocities, (b) particle turbulent fluctuations (Re = 64000, d_p=1 μm)

was negligible. In Figure 4.7(a), all three turbulent k-ε models gave identical velocity profile. The predictions are close to the measured data upstream of x/H = 5. At x/H > 5, the models clearly over-predicted the particle velocity. Similar results can be found in Figure 4.7(b): three models gave predictions that were higher than the experimental data downstream of x/H = 5. However, the standard k-ε model didn't predict the particles in the recirculation region while the other two models successfully predicted.

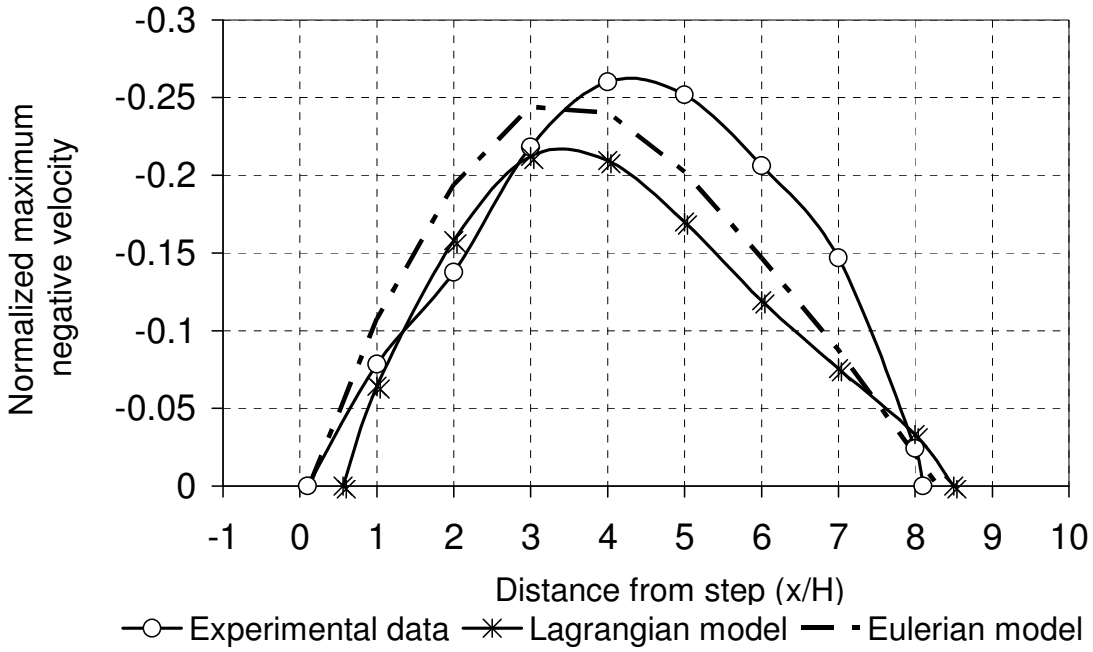

Figure 4.9 Maximum negative velocity U-max (normalized with Uo) in the recirculation zone of particles; Lagrangian and Eulerian models (Re = 64000, d_p=1 μm)

Figure 4.8 illustrate the particle velocity profiles and particle turbulent fluctuation respectively, obtained using the Lagrangian particle tracking and Eulerian two-fluid models for the flow condition of Re = 64000 and particles of diameter size of 1 μm. The model predictions have been attained through both methodologies employing the RNG k-ε turbulent model. Good agreement was achieved between the model results and measured data. A closer investigation revealed that the Eulerian model was, however, seen to provide better results than the Lagrangian approach especially near the geometry exit. Comparison of the numerical and measured profiles of the particle maximum negative velocity is presented in Figure 4.9. It is evidently clear that better prediction was achieved through the Eulerian model by the excellent matching of its predicted profile shape and reattachment length with the experimental profile. For small particles, the discrete random

walk model used in this study is with a deficiency. In strongly inhomogeneous diffusion-dominated flows where small particles should become uniformly distributed, DRW will predict high concentration in low-turbulence regions of the flow (MacInnes and Bracco, 1992).

Figure 4.10(a) shows the mean particle velocity profiles using the Lagrangian particle tracking and Eulerian two-fluid models for the flow condition of Re = 15000 and 70 μm particles. For these lower inertial particles, particle penetration into the recirculation zone was identified. For larger size particles in high Reynolds number flow, Lagrangian model predicted particle-free zone in the recirculation zone (also see Figure 4.7) while the Eulerain two-fluid model revealed particles entering the recirculation zone. Slater and Young (2001) explained that the cause was derived from the ill posedness of the particle equation of the Eulerian method where it saved all the information in the whole domain including the particle-free zone. However, it should be noted that the reported particle concentration using the Eulerian approach in the particle zone was decreasing with increasing particle size. When the particles were taken to 45μm, the particle concentration at the center of the recirculation zone dropped to about 1×10^{-5}. When the particle sample number was increased to 5×10^{4}, several particles were found to exist in the recirculation zone. Hence, the predictions of the Eulerian model were consistent with the Lagrangian model in as far as the particles were flowing in the particle-free zone. Figure 4.10 (b) presents the simulation and experimental results of particle turbulent fluctuation velocity profiles for flow condition of Re = 15000 and particle size of 70μm. The Lagrangian model significantly under predicted the particle turbulent fluctuation. Fessler et al. (1997) drew the conclusion that when k-ε turbulence computations were performed alongside with the Lagrangian particle tracking, the methodology was unable to properly account the interactions of the particle movement with the large-scale instantaneous flow structure. Another possible cause of error could be the absence of accurately quantifying the particle inlet fluctuation for the Lagrangian model.

Comparison of the maximum positive velocity profile between measurements and computations is demonstrated in Figure 4.11. Here, both models yielded identical results that were marginally higher than those measured.

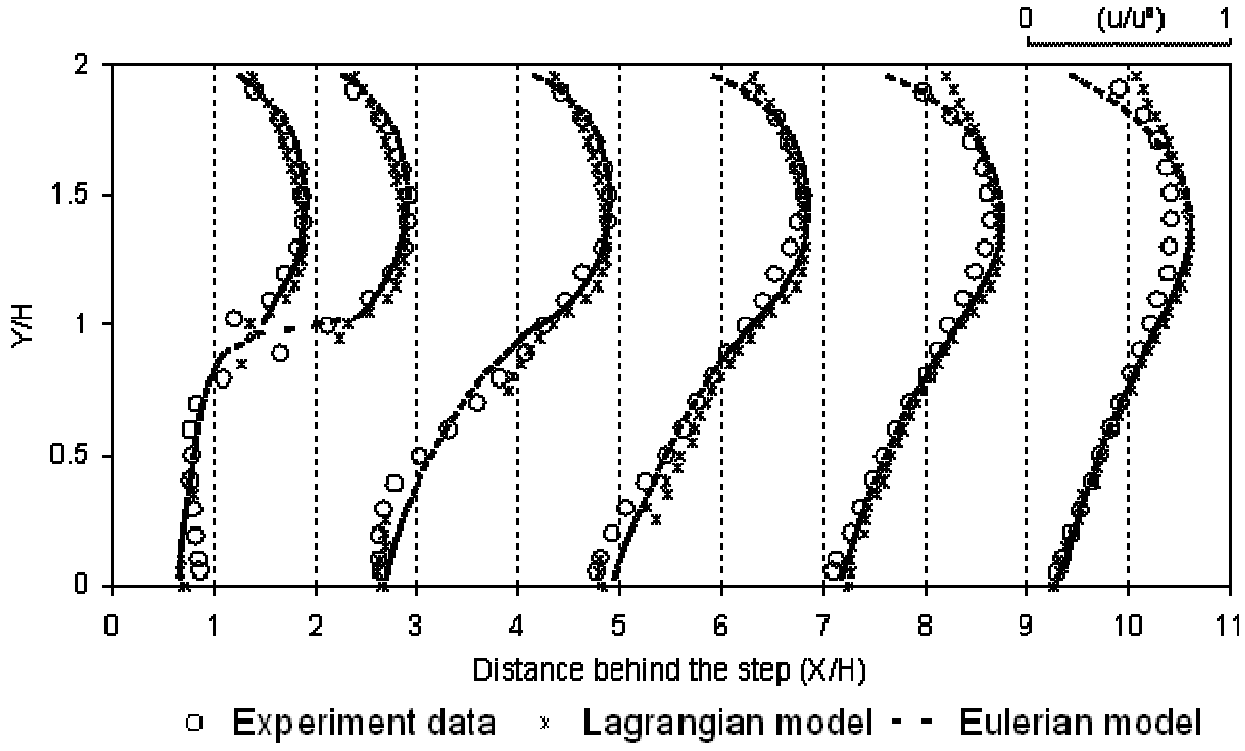

(a)

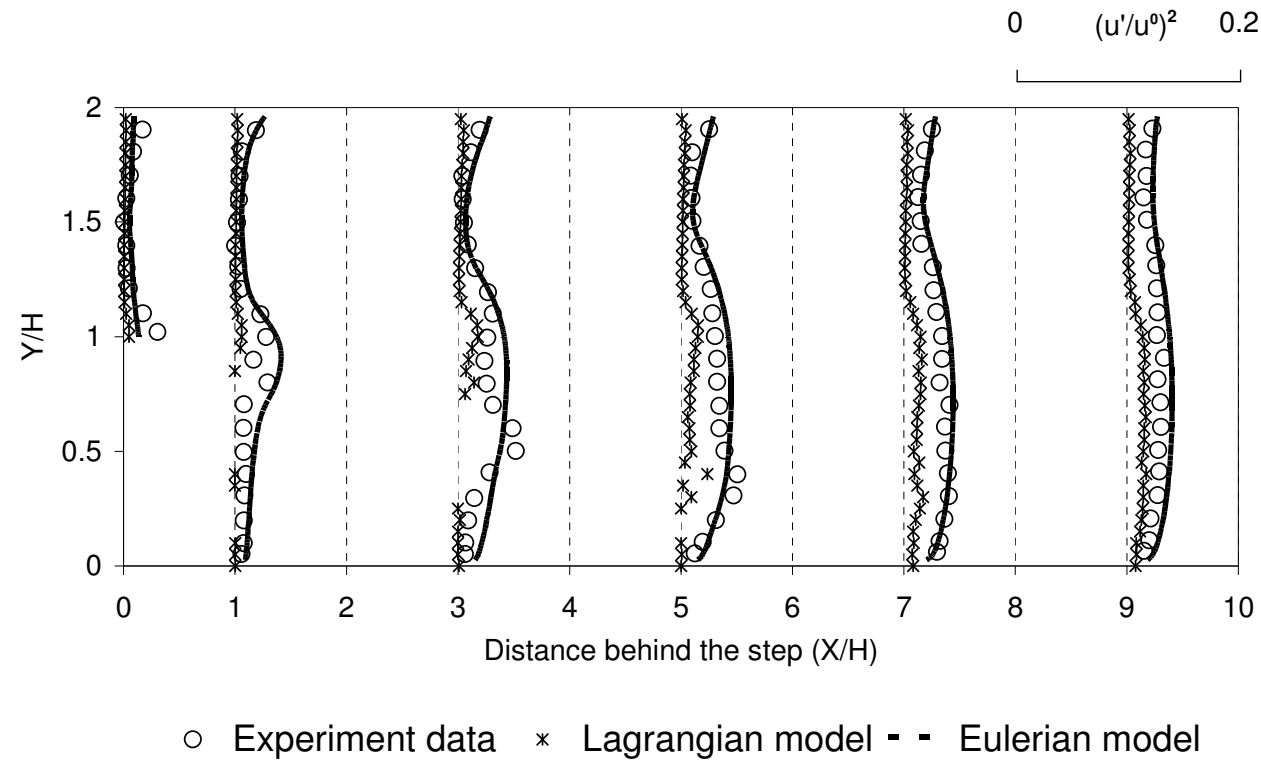

(b)

Figure 4.10 Comparison between the experimental data and numerical simulation results with Lagrangian and Eulerian models: (a) particle velocities, (b) particle turbulent fluctuations (Re = 15000, d_p=70 μm)

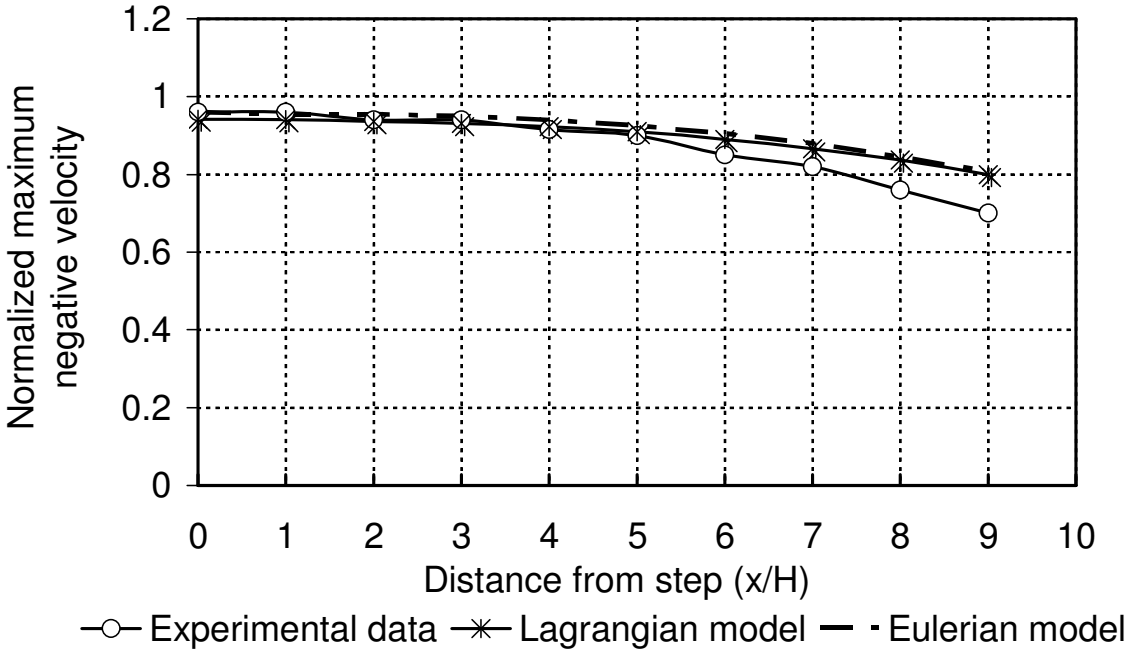

Figure 4.11 Maximum positive velocity U+max (normalized with Uo) in the streamwise portion of the velocity profile of particle (Re = 15000, d_p = 70 μm)

4.1.3 Summary

The physical behavior of a turbulent gas-particle flow over the backward facing step geometry was numerically investigated via a Lagrangian particle tracking model (DRW model) and an Eulerian two-fluid model combining with an overlapped grid technique (Tu, 1997). A substantial amount of work was undertaken in this paper to further elucidate the understanding of the particle flow under the influence of particle inertia (Stokes number). For the case where the particles acted like fluid traces (St << 1), the prediction accuracy of the gas phase turbulence was strongly affected by the application of turbulent k-ε models for the particular geometry concerned. For a backward facing geometry, the RNG k-ε and realizable k-ε models gave the better prediction especially for the particle reattachment length than the standard k-ε model. Similarly, for the flow of heavier particles (St >> 1), the RNG k-ε model and realizable k-ε were still seen to provide marginally better performance than the standard k-ε model. The computational results obtained by both the Eulerian-Lagrangian model and the Eulerian-Eulerian model were compared against benchmark experimental data. The comparison revealed that both approaches provided

reasonable good predictions of the velocities and turbulent fluctuations for the gas and particle phases. Nevertheless, the closer numerical investigation showed that this Eulerian-Eulerian model gave marginally better performance than the Eulerian-Lagrangian model. It also has been demonstrated that more computational time is required for Eulerian-Lagrangian approach than Eulerian-Eulerian approach. In engineering applications, the Eulerian-Lagrangian approach is recommended when the detailed physics for the particle phase are required. For complex flows that require large computational resources for the Lagrangian model, the Eulerian-Eulerian model is an attractive alternative.

4.2 Turbulent gas-particle flow in a 3-dimensional 90-degree bend

Gas-particle flows in curved ducts are commonly found in many engineering applications. Air-coal flows in coal combustion equipments, coal liquefaction-gasification pipe systems, gas-particle flows in turbo machinery, contaminant particle flows in ventilation ducts are just some typical examples. With the development of computer power and advancement of commercial modeling software, CFD technology has been used as an attractive tool to investigate particle-gas flows in curved ducts. Tu and Fletcher (1995) employed an Eulerian-Eulerian model to simulate a gas-particle flow in a square-sectioned 90° bend. This two-fluid model includes a set of Eulerian formulation with generalized wall boundary conditions and a particle-wall collision model to better represent the particle-wall momentum transfer. Comparison of both gas and particle phase velocities computations against the limited experimental measurements of Kliafas and Holt (1987) were reasonable good. Shimomizuki et al. (1993) investigated the gas-particle flows in a bend of rectangular duct using an Eulerian-Lagrangian model in which particle-wall collision was calculated by a semi-empirical model by Tabakoff (1984). Naik and Bryden (1999) computed the trajectories of particles with different diameters in a 90° bend using an Eulerian-Lagrangian model. They utilized a simple particle-wall impact model assuming that the normal and tangential restitution coefficients were 0.9 and 0.8 respectively. The commercial CFD package, FLUENT, was used by McFarland et al. (1997) to study the aerosol particles penetrating through bends. They tracked the particle trajectories via a ‘Random Walk’ model and assumed aerosol particles deposited when impacting the walls.

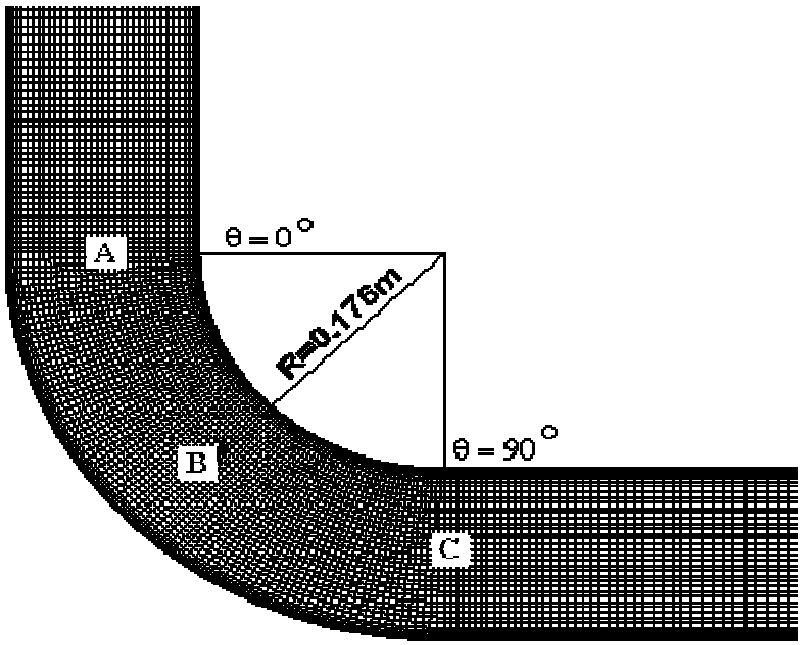

(a)

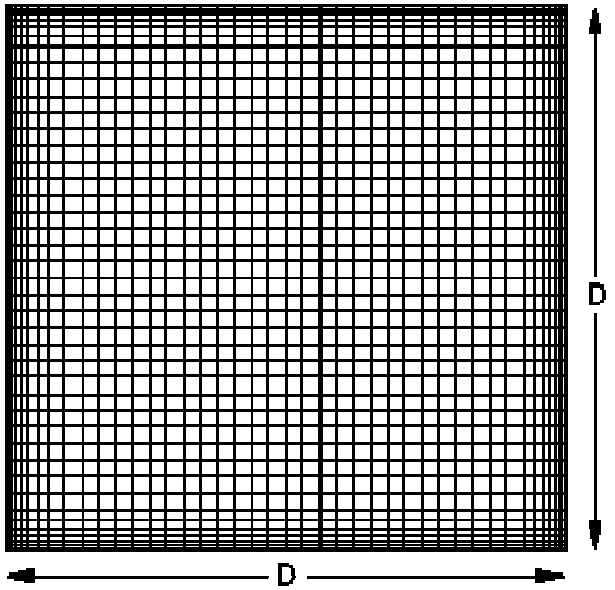

(b)

Figure 4.12 Computational domain for the 3-D 90 degree bend (a) bend and (b) inlet

The numerical studies of the turbulent gas-particle flow in a square-sectioned 90 degree bend using both the Eulerian-Lagrangian model and the Eulerian-Eulerian model (Tu, 1997) are presented. The simulation results of both the numerical approaches are compared against the experimental data (Kliafas and Holt, 1987).

4.2.1 Numerical procedure

In this study, particles are made of glass with a material density (ρ_p) of 2990 kg/m^3 and diameter size of 50 μm. A nonorthogonal boundary fitted coordinate grid was employed for the study. The sample grid used for the computations is illustrated in Figure 4.12. The computational domain starts 10D upstream from the bend entrance and extends up to 12D downstream from the bend exit; there is also a uniform distribution of 45 control volumes placed at every 2 degree interval along the bend.

The governing transport equations were discretized using a finite-volume approach. The equations were solved on a nonstaggered grid system. Third-order QUICK scheme was used to approximate the convective terms, while second-order accurate central difference scheme was adopted for the diffusion terms. The velocity correction was realized to satisfy continuity through SIMPLE algorithm, which couples velocity and pressure. Uniform velocity was imposed at the top inlet plane of the bend with wall boundary conditions imposed on the top and bottom and also along the sides of the 90^o square duct. The computational domain remains the same for both the approaches. The particle-wall collision model of Sommerfeld (1992) was used for the Eulerian-Lagrangian model but the wall roughness effects were not considered in the current case. Chapter 6.2 presents a more detailed investigation into effects of wall roughness on the gas-particle flow in a 90-degree bend that has the same geometry as the current one but is two-dimensional.

4.2.2 Results and Discussions

The mean quantities of both the gas and particulate phases i.e., their velocity, concentration and fluctuation distributions along the bend are compared, as mean quantities are of utmost interest in engineering applications. The results obtained from both approaches were

recorded from the mid plane of the duct geometry. All the values reported here (unless or otherwise stated) are normalized using the inlet bulk velocity (u_0=52.19 m/s).

Figure 4.13 presents the predicted pressure distribution on the duct middle plane. In the region of the inner wall of the bend entrance, an initially favorable (positive) longitudinal pressure gradient existed, while an unfavorable (negative) longitudinal pressure gradient presented near the outer wall of the bend entrance. The presence of the favorable and unfavorable pressure gradients was caused by the balance of centrifugal force and radial pressure gradient in the bend.

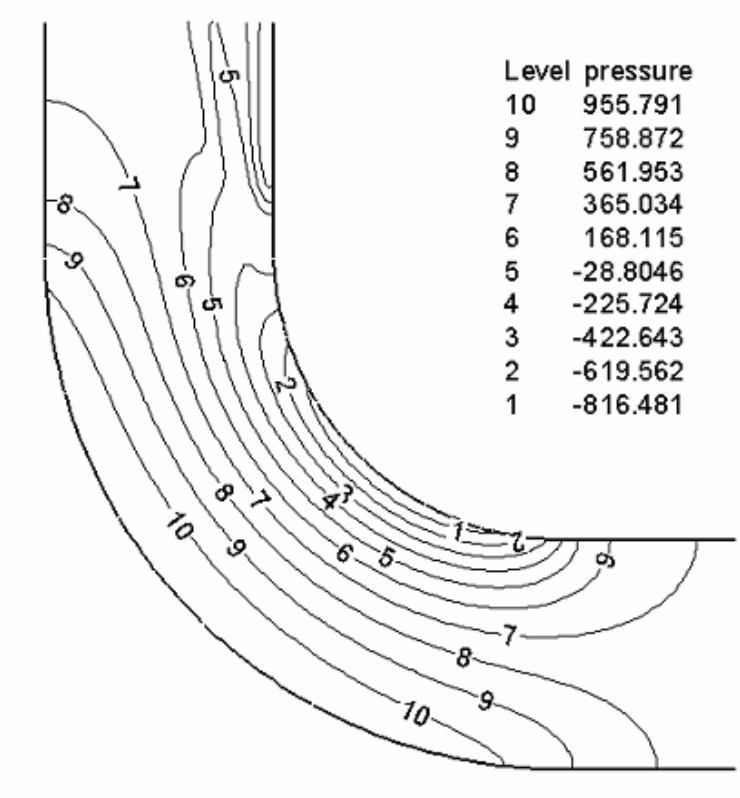

Figure 4.13 Calculated static pressure distribution

Figure 4.14(a) shows the comparison of the numerical results against the experimental data for means streamwise gas velocity along various sections of the bend. It can be seen that there is a good quantitative comparison with both numerical models against the data from Kliafas and Holt (1987). At the entrance of the bend, the numerical simulation successfully predicted the acceleration of the gas phase near the inner-wall. In the region near the outer wall, the fluid deceleration caused by the unfavorable pressure gradient was also captured. The predictions of streamwise turbulence intensity of the carrier phase in the Eulerian and

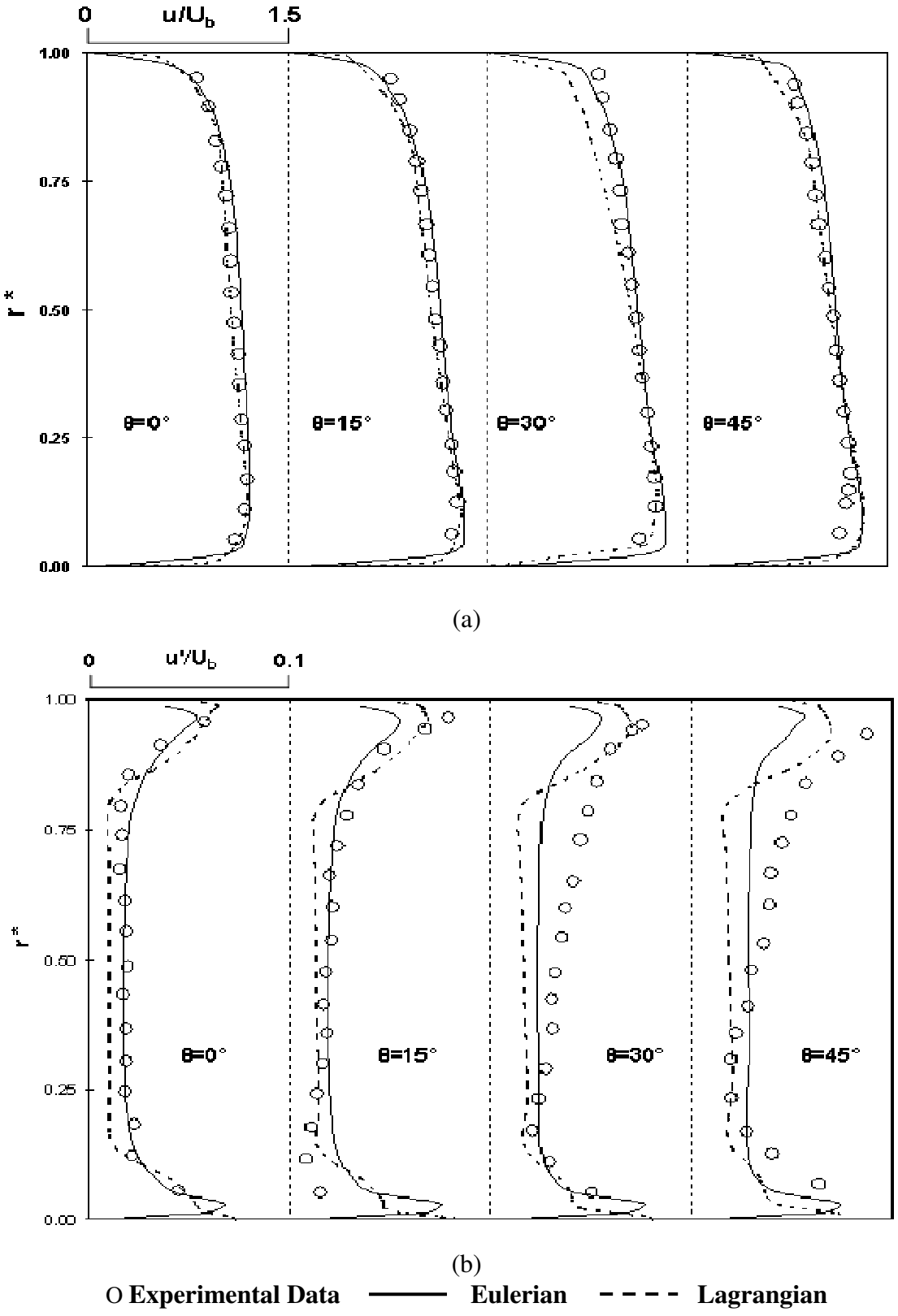

Figure 4.14 (a) Mean streamwise gas velocities along the bend; (b) Mean streamwise gas turbulence along the bend

Lagrangian models are compared in Figure 4.14(b), wherein a very small Stokes number of

particle phase was used as the seed. High turbulence intensity can be seen near the walls, due to high shear rate, when compared to the core region of the flow. There was a general under prediction by both methods towards the outer wall in the 30 & 45 degree sections.

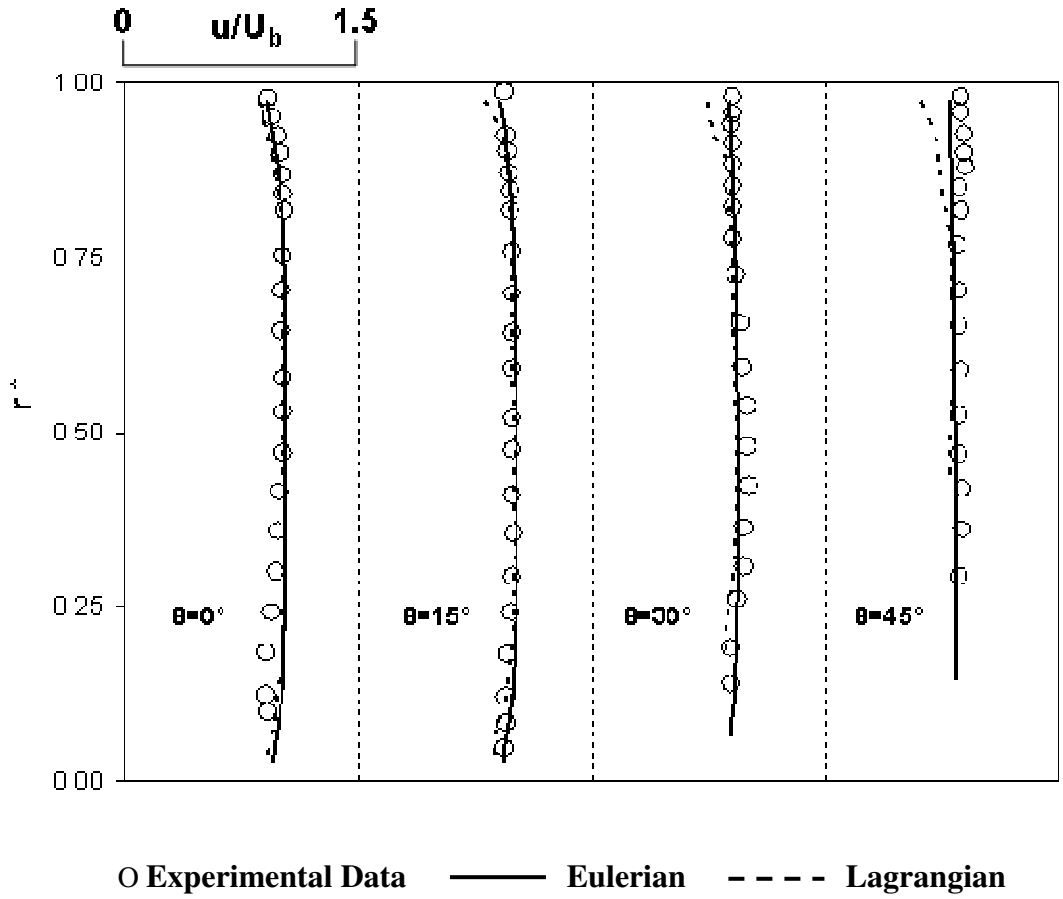

Figure 4.15 Mean streamwise particle velocities along the bend

Figure 4.15 shows the comparison of mean particle velocities; it is evident that there is a generally good agreement between the experimental and predicted data using both Eulerian and Lagrangian numerical approaches. The Stokes number for the experimental case was found to be about 12.87 (i.e., St>>1) and there by flatter profiles were noted for the dispersed phase. This proves that they are not affected by gas pressure gradients. It can also be observed that the particle velocities are lower than the fluid velocities. This is similar to the observations made by Kulick et al. (1994) where the particles in the channel flow show a negative slip velocity due to cross-stream transport.

In order to better understand the particle behavior around the carrier gas phase, further simulations for various Stokes numbers were presented using Eulerian two-fluid formulation against the carrier gas phase velocity. It can be seen from Figure 4.16 that

particles act as 'gas tracers' for a Stokes number of 0.01 as they are found be fully in equilibrium with the carrier phase and this phenomenon becomes less pronounced as the Stokes number is increased. It can also be seen from the 0 and 45 degree bend sections that there exists a positive slip velocity between the particulate and gas phase at the outer walls along with the velocities of the gas peaking at the inner walls due to the presence of a favorable pressure gradient. This 'gas tracing' phenomena of the particles become less pronounced as we approach the bend exit, as the flow regains the energy it lost due to slip. It can also be observed that for flows with St $\geq$ 1 the positive slip velocity between the particle and gas velocity keeps decreasing along with the bend radius and turns negative at the bend exit where the gas leads the particle. This is attributed to the fact that the particles are not able to keep up with the gas due to its own inertia in addition to its energy loss attributed towards particle wall collisions. To understand the particle paths along the bend for the above cases of Stokes number, their paths using Lagrangian formulation are depicted in Figure 4.17, it can be seen that as the Stokes number is increased the particles show a general movement towards the outer bend.

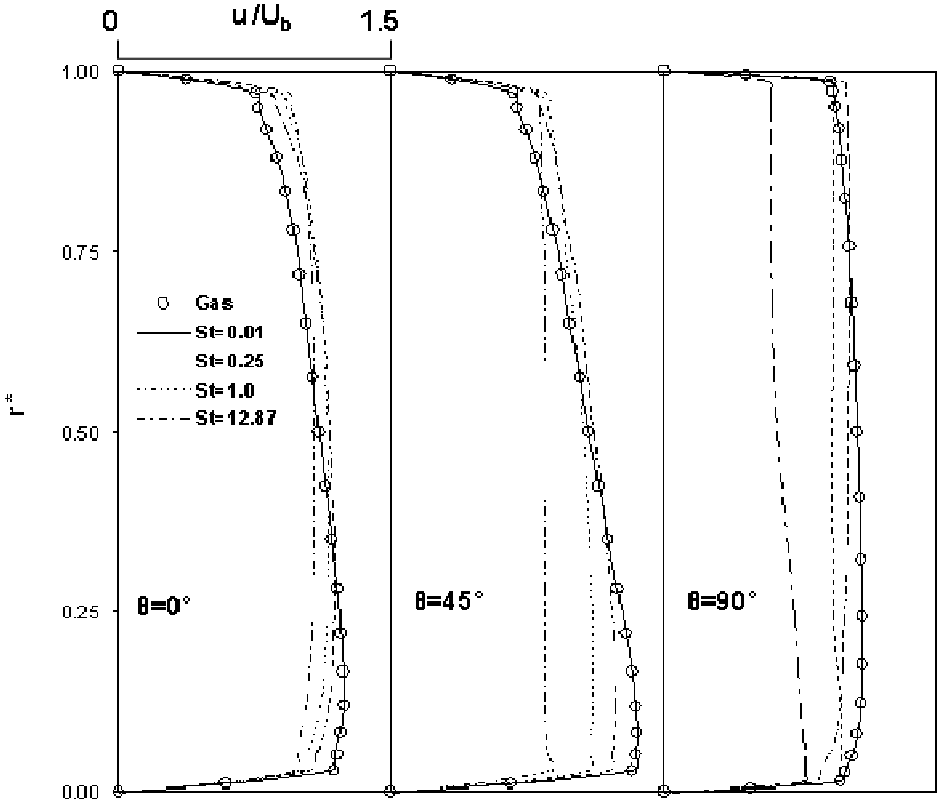

Figure 4.16 Streamwise velocities along the bend for varying Stokes number.

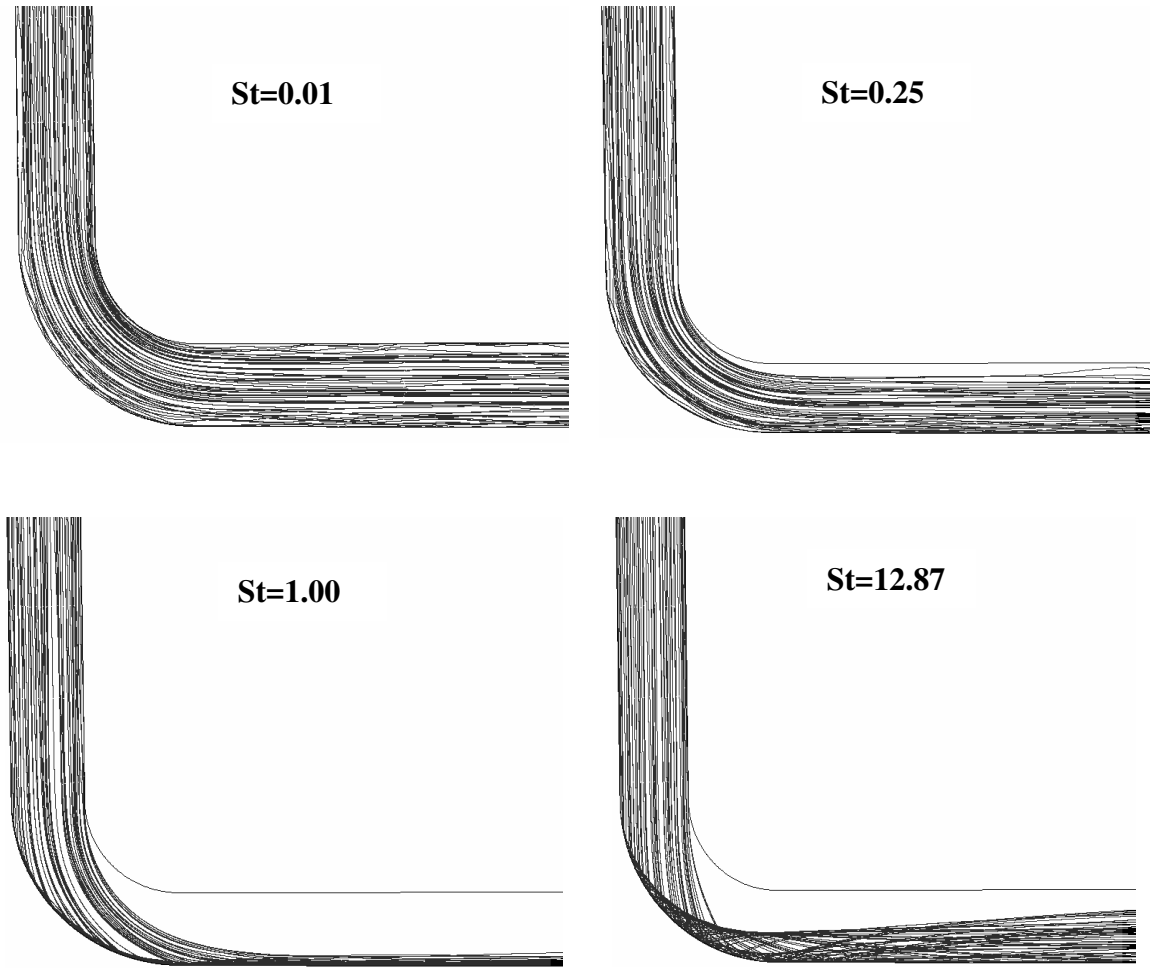

Figure 4.17 Lagrangian particle paths for varying Stokes number.

4.2.3 Summary

The current study investigated the turbulent particle-laden flow in a square sectioned 90^{o} bend through the comparison made by two approaches: Eulerian two-fluid model and Lagrangian particle tracking model (DRW model). The computational results were compared against the benchmark experimental data. The results revealed that both approaches provided reasonably good comparison for gas and particle velocities together with the fluctuation for the gas phase. For the particle concentration distribution along the bend, a remarkable qualitative agreement with the measured data has been shown using the Eulerian-Eulerian model. The Eulerian-Eulerian model provided useful insights into the particle concentration and turbulence behavior when compared to the Eulerian-Lagrangian approach, while Eulerian-Lagrangian model can give detailed particle trajectories.